Chirality in double photoemission from a Cu(100) surface (EP)

F. O. Schumann, G. Di Fillippo, Z. Wei, et al.

COLLECTIONS

Paper published as part of the special topic on Commemorating the Career of David Arthur Shirley

EP   This paper was selected as an Editor's Pick

openaccess

View Online   Export Citation   CrossMark

ARTICLES YOU MAY BE INTERESTED IN

Chirality in double photoemission from a Cu(100) surface 〔EP〕

F. O. Schumann,[1,a)] G. Di Fillippo,[2] Z. Wei,[1,b)] and G. Stefani[3]

AFFILIATIONS

[1]Max-Planck-Institut für Mikrostrukturphysik, Weinberg 2, 06120 Halle, Germany
[2]CNISM and Dipartimento di Scienze, Università Roma Tre, via della Vasca Navale 84, 00146 Roma, Italy
[3]CNR-ISM, Via Fosso del Cavaliere 100, 00133 Roma, Italy

Note: This manuscript is a part of the Special Topic Collection Commemorating the Career of David Arthur Shirley.
[a)]**Electronic mail:** schumann@mpi-halle.de
[b)]**Present address:** College of Materials Science and Engineering, Chongqing University, 400044 Chongqing,
People's Republic of China.

ABSTRACT

We investigated the double photoemission process from a Cu(100) surface with circular polarized light using coincidence spectroscopy. The handedness of the photon can be imprinted onto the emitted electron pair. The proof of this assertion lies in a helicity dependence in the electron pair intensity. We selected a photon energy that allowed the emission of the $3p$ core electron. Therefore, we recorded coincidences from the $3p$ electron and associated Auger electron. An additional pathway of double photoemission is the absorption of the photon by the valence band without the participation of a core electron. Adopting a chiral detection geometry, we were able to observe nonvanishing dichroism signals in both pathways of double photoemission. Hence, the emitted electron pair is chiral. Furthermore, the existence of this effect in our geometry implies that the Auger decay upon Cu $3p$ excitation proceeds in a single step.

I. INTRODUCTION

Double photoemission (DPE) is the ejection of an electron pair due to the absorption of a single photon. This possibility was already anticipated in the landmark paper of Einstein.[1] If the emitted electrons originate from the valence band and there is no core-level participation, we call this process direct DPE. If the photon energy is sufficiently high, a core electron can be liberated. The filling of the core vacancies leads to the emission of an Auger electron. The rearrangement of electrons may lead to two vacancies in the valence band; in this case, we talk about core-resonant DPE.

It is well established that single photoionization of unpolarized atoms is insensitive to the helicity of the incident photon and no difference is observed between photoemission spectra obtained with left or right circular polarization. This is because the initial atom and the final ion have no preferred orientation and no chirality is introduced in the experimental setup. Nonetheless, it is possible to observe chiral effects in single photoemission by constructing an asymmetric experimental setup. This can be done, e.g., by resolving the spin of the emitted electrons in spin–orbit coupled systems. Here, the oriented reference system is determined by the wave-vector of the photon, the momentum of the photoelectron, and spin projection. Analogous effects can be observed in naturally polarized targets, e.g., magnetized samples, for which dichroism in the photoemission spectrum can be achieved by reversing the magnetization of the sample.

In the case of electron pair emission via single photon absorption, the helicity of circular polarization enters in a nontrivial way in the definition of the cross section of the process. In order to observe a finite DPE intensity (regardless of the polarization state of the photon), a nonvanishing electron-electron interaction is needed.[2–4] This is determined by the Coulomb interaction between electrons. The description via effective single electron states will result in a vanishing intensity. This means that it is mandatory to use correlated wave functions that are not a product of single electron states. This has the consequence that the photon is absorbed

by an electron pair, despite the fact that the photon-electron interaction is mediated by a single electron operator.[3] This emphasizes the potential of DPE to unravel the details of the electron-electron interaction. It is stressed that the DPE process is inherently a single-step process.[3,5,6]

Since the circular polarized photon is absorbed by the electron pair and the target initial state is achiral, one can think that the photon chirality in the final state is transferred to the two interacting electrons.[7] This means that, due to the electron correlation, the electron pair possesses a chirality as an internal degree of freedom that can be probed by varying the helicity of the photon.

This concept was first theoretically discussed[7,8] for the He atom, with the prediction of a helicity dependence of the cross section for electron pair emission. This is at first glance surprising because the He atom is in an isotropic ground state and no spin resolution is considered and also single photoelectron emission displays no helicity dependence.[7,8] The validity of the concept was demonstrated in a few coincidence experiments on the He atom.[9–11] The key ingredient for the observation is to introduce a handedness in the experimental geometry.[7–9]

In core-resonant DPE, a core-photoelectron, together with an Auger electron, is emitted. An often-made approximation is to assume that the Auger decay occurs significantly later after the core-electron ejection. In this case, one can treat the two processes separately, leading to a two-step picture.[5,6] The helicity dependence on the core-resonant DPE process within this approximation was also theoretically discussed.[12] It was predicted that a dichroic signal is present and that the detection requires a chiral geometry as in the one-step DPE.[12] One important difference between a one-step and a two-step picture concerns the dependence on the angle between the emitted electron trajectories.

In the He atom, no electrons are left behind in the atom after double ionization that could carry the photons' chirality. This is not the case for atoms with $Z > 2$ and for a solid. It is not clear whether averaging over the undetected degrees of freedom of the left-behind sample would wash out the helicity-dependent correlations between the two ejected electrons. Furthermore, we have chosen a Cu(100) surface and have tuned the photon energy such that the $3p$ core electron and associated Auger electron are emitted. This allows us to observe core-resonant and direct DPE under the same experimental conditions. As far as the core-resonant DPE is concerned, we have identified it to be a single-step process.[13] In this work, we demonstrate that the core-resonant DPE process exhibits dichroism in energy spectra. It is confined to the spectral region of the ^1G 2-hole final state multiplet, while the region covering the ^3F term is unaffected by the helicity of the light. Given the geometry of our setup, the detection of a core-resonant dichroism is additional proof that the core-resonant process involving the Cu $3p$ level must be a one-step process. For the direct DPE process, we can also detect this, but the signal strength is much weaker in this process.

II. EXPERIMENT

We employed a setup explained in some detail elsewhere.[13–16] The key components are a pair of hemispherical analyzers with 200 mm mean radius, which we call "left" and "right," respectively.

They feature at their exits channel plates as electron detectors. These are equipped with resistive anodes which allow us to record the impact position on the channel plate. This, in turn, provides the kinetic energy information. We employ a four-way coincidence circuit in which the channel plate signals have to be within 185 ns, while at the same time, the electronics of the resistive anodes indicate a successful impact position determination. For each valid event, the arrival time (t_{left} and t_{right}) at the respective detector with respect to the coincidence trigger is known. The computation of the arrival time histogram $dt = t_{left} - t_{right}$ shows a peak residing on a constant background. The peak is the evidence of the "true" coincidence. We follow established procedures to remove the contribution of "random" events, and all spectra we present have been corrected in this way.[14,17–20]

In order to be sensitive to a dichroic effect with circular polarized light, the geometry of the experiment has to be appropriately chosen.[7–9] First, the emitted electrons must be detected in coincidence; second, both electrons must possess different kinetic energies. Furthermore, the emission direction is neither back-to-back nor parallel. Finally, the photon propagation direction does not lie in the plane defined by the escaping electrons. In simple terms, the two emission directions and the helicity vector of the photon introduce a handedness. The listed conditions are necessary but are not sufficient for the detection of dichroism.

In Fig. 1, we show the overall alignment of the spectrometer and photon beam fulfilling this requirement. The electro-optical axes of the two spectrometers are perpendicular to each other. Within this scattering plane, the angular acceptance is ±15° and the photon beam is perpendicular to the scattering plane. The dichroic signal scales with $\sin(\alpha)$, where α measures the angle between the photon propagation direction and the scattering plane.[7] Consequently, our geometry is expected to give the maximum dichroic signal as far as the alignment of the scattering plane with the light propagation is concerned. It is *a priori* not clear which angle between the spectrometer will provide the highest signal. At any rate, the setup is constraint to allow only a perpendicular orientation between the two lens axes. In this case, a two-step process will yield a vanishing dichroism[12] in contrast to the one-step process.[7,12]

The sample manipulator axis is within the x–z plane such that the incoming light has a grazing angle of 10° with the [010] direction of the Cu(100) surface. The surface normal **n** has an angle of 45° with respect to the spectrometer aligned along the x-axis. Due to the small tilt of the manipulator axis from the z-axis, the vector **n** has an angle of 45.9° with the y-axis. Strictly speaking, the emission geometry is not symmetric, but the deviation is small.

The energy dispersive properties of a hemispherical analyzer are well-documented in the literature.[21,22] The energy window captured by such an analyzer is given by the mean radius, the diameter of the channel plate, and the pass energy. For the dimensions of our instrument and detector, one finds that 9% of the pass energy is dispersed onto the detector.

All experiments were performed with the pass energy set to 300 eV. Hence, an energy window of 27 eV is captured by the detector. The selected slit size lead to an energy resolution of 0.8 eV. We kept the settings constant for a measurement of a given photon energy. All kinetic energies are referred to the vacuum level
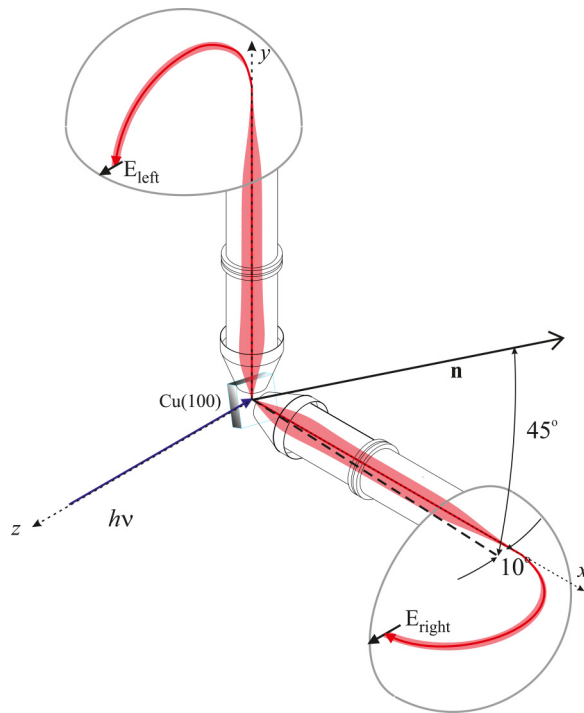
FIG. 1. Two spectrometers define a scattering plane and the electron-optical axes of the spectrometer are perpendicular to each other. They define x- and y-axes. The propagation direction of the UV radiation is along the z-axis. The manipulator axis is within the x–z plane tilted by an angle of 10°. The surface normal **n** of the sample encloses an angle of 45° with the x-axis (Ref. 13). The perpendicular arrangement of the photon beam to the scattering plane is anticipated to give maximum chiral dichroism for given spectrometer orientation (Ref. 7). Reproduced with permission from van Riessen et al., J. Phys.: Condens. Matter **22**, 092201 (2010). Copyright 2010, IOP Publishing. All rights reserved.

of the sample, and the sample was at room temperature during the measurements. The preparation of the Cu(100) surface followed standard procedures of Ar^+ sputtering and annealing. The base pressure of the chamber was 5×10^{-11} mbar. The experiments were performed at the undulator beam line UE56/2-PGM-2 in the multibunch mode of the BESSY II electron storage ring at the HZB/Berlin. This beamline can provide linear polarized light along two orthogonal directions and circular left/right polarized light.[23,24] The characterization of this beamline demonstrates a degree of circular polarization close to 100%. We performed measurements with circular polarized light and a photon energy of 125 eV. The total acquisition time was 6.1 days, and the number of coincidence counts are around 250 000.

As it is customary for coincidence experiments, one has to strongly reduce the primary flux compared to single electron spectroscopy. We operated with a singles rate of about 2500 cps on each spectrometer. The chosen primary flux resulted in a ratio of "true" to "random" coincidences of 3.2, while the coincidence rate was 0.47 cps. The helicity was changed in regular intervals. We ensured that the singles, coincidence count rates, and the "true" to

"random" ratio stayed the same. Hence, we arrived at almost exactly the same number of accumulated counts for both helicities.

III. RESULTS

Strictly speaking, an Auger emission always result from a one-step core resonant DPE. Nonetheless, when the core hole lifetime created by the photon absorption is sufficiently long lived, the two-step model becomes an efficient approximation.[5,6]

This means the Auger electron emission can be treated separately from the photoelectron emission. Other than the requirement of energy conservation, the energies of the two emitted electrons do not depend on each other. Nevertheless, there is still a relation between the two electrons because of the selection rules for the photo and Auger electron transition.[25,26] This causes the Auger line shape to be affected by the emission direction of the photoelectron.

In an one-step process, one has to describe the emission of an electron pair rather than the individual electrons. This has the consequence that there is a relation between the emission energies beyond energy conservation. We have previously discussed how these two pathways lead to very different 2D-energy distributions within a model.[27,28] The inputs for this description are single electron spectroscopic data, e.g., Auger kinetic energy and binding energy of the core level together with their linewidth.[29,30] Assuming a photon energy of $h\nu = 125$ eV and a work function of $\phi = 4.6$ eV[31] for the Cu(100) surface, we obtain Fig. 2. The energy of the Auger and photoelectron are 57 and 46 eV, respectively. In the case of a two-step process, the intensity is confined in regions parallel to the energy axis as observed in coincidence experiments.[27,28,32–35]

A one-step process is characterized by a diagonal intensity band that keeps the energy sum constant. This is the case for the Auger decay of the Cu 3p as shown in Fig. 3(a). This is not an isolated situation because this kind of behavior is also seen in the core-resonant process of the 4p level of Ag and Pd.[27,28] The underlying physics is the rapid fluctuation of two configurations after
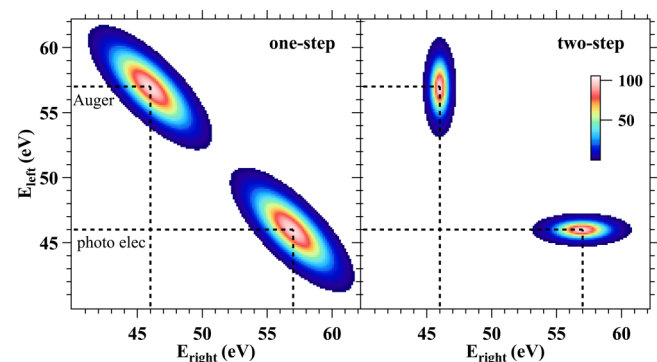

FIG. 2. Schematic 2D-energy distribution for a one-step and two-step core-resonant DPE process as described in Refs. 27 and 28. The inputs for this sketch are single electron spectroscopic data, see the text. The photon energy is set to 125 eV, while the work function is 4.6 eV. The dashed lines mark the energetic position of the Auger and photoelectron.
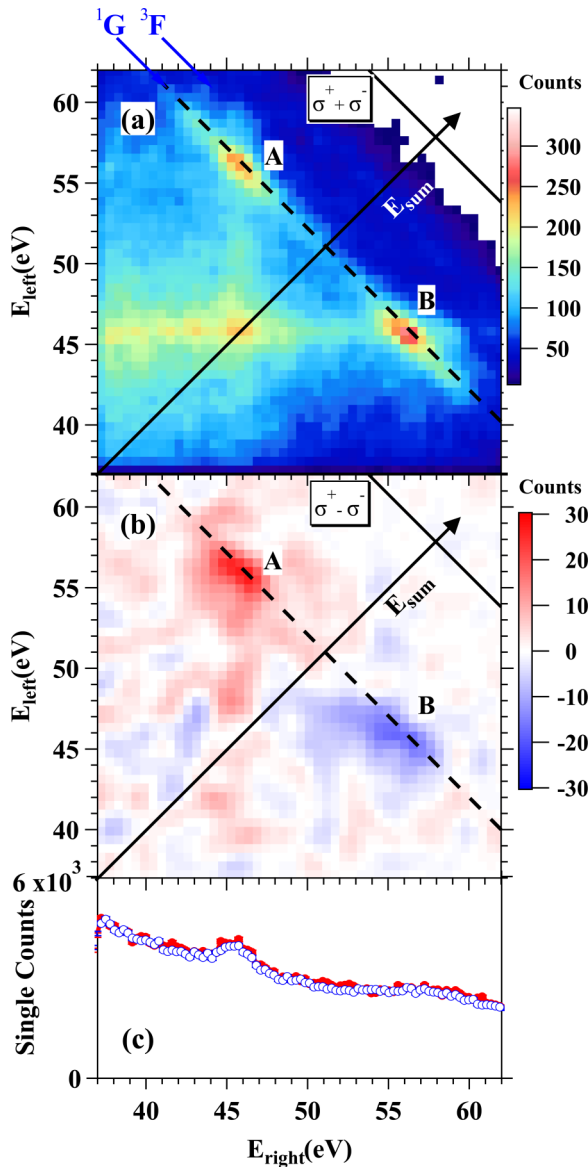
FIG. 3. In (a), we show the 2D-energy distribution integrated over both helicities $\sigma^{\pm}$. The photon energy was 125 eV. The solid diagonal lines marks the E_{sum}^{max} line. The blue arrows indicate the ^1G and ^3F positions. High intensity pockets are labeled with A and B, which are connected by a dashed line. A bisecting line/arrow indicates the E_{sum} direction for data points on this line $E_{left} = E_{right}$. (b) shows that the difference spectrum and a dichroic effect along the core-resonant ^1G diagonal is clearly resolved. The single electron spectra (c) do not display a dependence on the polarization. The red (blue) data points refer to $\sigma^+(\sigma^-)$. For a colored presentation of this figure the reader can refer to the web version of this article.

photon absorption.[36] The peak positions of the Auger and photo-electron are the same for the one-step and two-step processes. Hence, single electron spectroscopy cannot discriminate between the two outcomes in contrast to coincidence spectroscopy.

As stated above, two DPE pathways exist in which a single photon lead to two holes in the valence band. The existence of the direct DPE pathway requires the presence of a finite electron-electron interaction. Furthermore, this interaction has to be treated beyond an effective single electron picture to provide a finite DPE intensity.[2,3] As a matter of fact, the direct DPE intensity can be linked to the electron correlation strength.[37] Supporting this notion was the experimental observation of a strong material dependence of the DPE signal. It was found that those materials that are termed highly correlated exhibit the highest DPE intensity.[38,39]

In the core-resonant DPE, the electron-electron interaction also plays an important role. This can be seen by recalling that the matrix element for the Auger electron emission includes the Coulomb interaction between the states involved in the transition.[40] This aspect can be experimentally observed by the kinetic energy of the Auger electron. The measured value can be compared with the value expected on the basis of the binding energy of the participating states. Any shift between the two values can be cast into a term usually labeled with U_{eff}.[41] This term can obtain sizeable values and in the case of Cu, $U_{eff} = 8\,eV$ is reported.[41,42] This effective electron-electron strength is the input for detailed Auger line shape analysis within the Cini–Sawatzky theory.[40,43]

Regardless of the actual pathway, we can define the maximum of the sum of the kinetic energies of the electron pair as $E_{sum}^{max} = h\nu - 2\phi$. The term ϕ is the work function of the sample and has to be accounted twice because two electrons leave the sample. We use a value of $\phi = 4.63\,eV$ for the Cu(100) surface.[31] We use the term E_{sum}^{max} as a reference energy for the presentation of energy spectra. If we take the difference $E_{sum}^{max} - E_{sum}$, we obtain the two-particle binding energy E_B^{2e} in analogy to the procedure in single electron spectroscopy. Next, we recall the key points of the quasiparticle band structure of Cu. The density-of-states (DOS) of the Cu valence band is characterized by a region of high values for the binding energy region from 2 to 5 eV below E_F. In total, there are 10 3d electrons. The 4sp band provides an almost constant contribution from about 9 eV below up to E_F. This is much lower than those from the 3d band because the occupancy is 1 electron.

We display in Fig. 3(a) the 2D-energy distribution obtained with $h\nu = 125\,eV$. The data for helicity σ^+ and σ^- have been added for this plot. We have included the E_{sum}^{max} position as a solid diagonal line. A bisecting arrow shows the sum energy direction. We notice almost no intensity near the E_{sum}^{max} line. This is a consequence of the low DOS of the strongly dispersing 4sp band. The main intensity can be found along the dashed diagonal line at the pockets labeled with A and B, respectively. In order to identify the energetic positions, one has to refer to available spectroscopy data that reveal the kinetic energy of the Auger electron and the binding energy of the core level.[29,44] In our work, we used the binding energy values for the 3$p_{1/2}$ and 3$p_{3/2}$ level as 77.1 and 74.9 eV, respectively.[45] The lifetime broadening of these two levels is almost the same as the spin–orbit splitting.[46] Due to the combination of the selected energy resolution of our spectrometer with the lifetime broadening, we observe essentially the peak position of the 3$p_{3/2}$ level. With this information, it is straightforward to identify that the coordinate 46 eV refers to the 3p photoelectron, while 57 eV identifies the Auger transition.

We label the sum energy position of the main intensity as ^1G, while a second region is identified as ^3F. These are multiplet designations of the two hole states which we discuss later. Clearly, the intensity is dominated by the contribution of the core-resonant DPE. We also notice that there is a weak diagonal intensity band connecting pockets A and B, which also extends to the region outside A–B segment. This we have discussed in an earlier work, and it constitutes a signature that the core-resonant process for the Cu $3p$ case proceeds in a single step.[13]

The experimental data are the counterpart of the simplified one-step sketch in Fig. 2. Not included in the cartoon is the contribution from the direct DPE. We have previously studied the DPE process from Cu surfaces with a photon energy, which was too low to excite the $3p$ level.[47–50] Hence, the energy spectra include only the direct DPE pathway. The 2D-energy spectra were rather broad, we will show below that the intensity above the dashed diagonal line of Fig. 3(a) comes from direct DPE.

In Fig. 3(a), we notice intensity rims emanating from the pockets A and B which are parallel to E_{left} and E_{right} axes. These rims cross each other if both energies are equal to 46 eV and lead to an intensity peak. Energetically they refer to two Cu $3p$ photo electrons, but this would constitute a "random" coincidence. As stated in the Experiment section, we are able to remove the "random" contribution. Therefore, the intensity lines indicate a coincidence between a photoelectron and an Auger electron where the latter has suffered an energy loss.

We also note that there is an asymmetry with respect to the bisecting line. We associate this with an imperfect alignment of the spectrometer axis with respect to the emission spot on the sample. In the present study, it turned out that the detection efficiency of the "left" spectrometer for the lowest energies is significantly reduced compared to the "right" spectrometer. This explains the weaker intensity of the vertical 46 eV intensity rim.

In Fig. 3(b), we show the 2D-energy distribution of the difference spectrum $\sigma^+ - \sigma^-$. At the position of the intensity pockets A and B, we clearly observe a dichroic effect. At pocket A, positive values are attained, while pocket B shows negative values. In these regions, the kinetic energy of the two electrons are different by an amount that can be controlled by the choice of the photon energy. Once the electron energies are different, the theory predicts a dichroic effect and a sign reversal as shown in Fig. 3(b).[7,8]

In Fig. 3(c), we plot the single electron spectrum from the *right* spectrometer for the two helicities. More precisely, we used the coincidence data but ignored the available information about the energy of the electron recorded with the *left* spectrometer. In other words, we integrated over all energies E_{left} within the coincidence dataset. The single electron spectra line up almost completely as predicted by the theory.[7,8] The small difference between the curves is caused by slight variations in the flux. However, the key feature of Fig. 3(b) is the redistribution of intensity, which causes a positive value for pocket A, while at pocket B, a negative value is observed. This is not caused by intensity variations, hence, the result in Fig. 3(b) is genuine and not due to instrumental instabilities.

We want to present the data of Figs. 3(a) and 3(b) via one-dimensional two-particle binding energy plots. In both cases, we will use the energy sum as the x-axis. This axis is drawn as a

bisecting arrow in Figs. 3(a) and 3(b). As stated above, we will use E_{sum}^{max} as reference; hence, we will use the two-particle binding energy E_B^{2e} as the axis. For each pixel in Fig. 3(a), we can compute the E_{sum} value and the intensity level filled into a histogram. This leads to the curve shown in Fig. 4(a). The y-axis is labeled as *Sum* because we added the intensity for both helicities.

This spectrum allows the identification of the core-resonant and direct DPE part. The region from $E_B^{2e} = 0-11$ eV refers to the direct part, while the part below $E_B^{2e} = 11$ eV designates the core-resonant part. The peak at $E_B^{2e} = 13.8$ eV is identified as the ^1G multiplet, whereas the ^3F term appears only at a shoulder
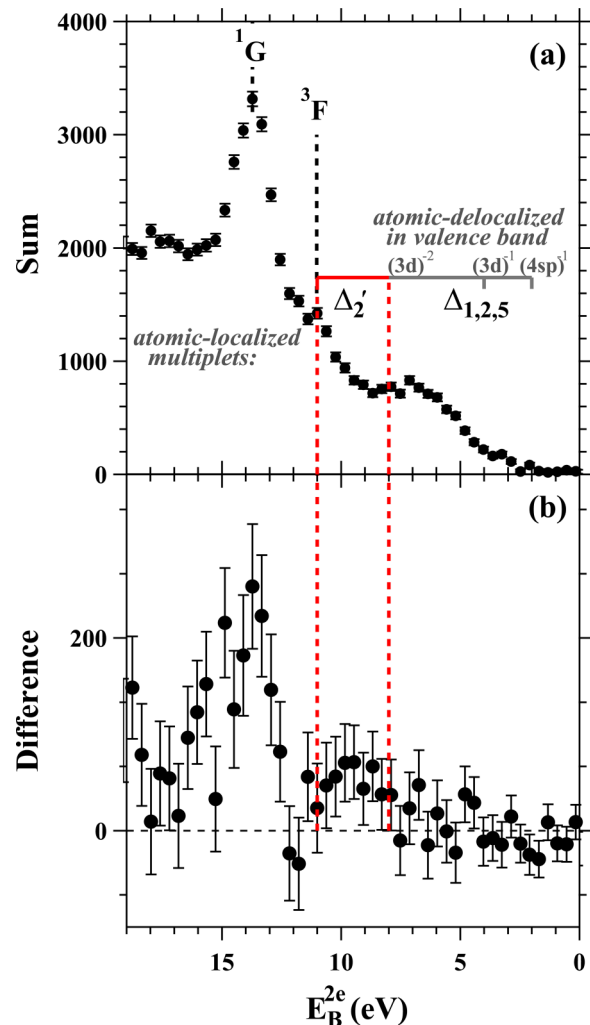
FIG. 4. In (a), we show the helicity integrated intensity spectrum as a function of the two-particle binding energy E_B^{2e}. The peak positions of the ^1G and ^3F terms are included. The spectral range above the multiplet is labeled according to the spatial symmetry of the band structure. In (b), we plot the helicity difference or dichroism spectrum as a function of E_B^{2e}. A dichroism signal from the ^1G peak and the $\Delta_{2'}$ spectral range can be observed.

around $E_B^{2e} = 10.8$ eV. The designation and energetic position is in line with the previous work.[46] The simplest approximation to describe the E_{sum} spectrum for DPE is to compute the self-convolution of the valence density of states. This curve has an almost triangular shape with a peak at $E_B^{2e} = 6$ eV.[50,51] Compared to this, the peak position of the ^1G peak is shifted by about 8 eV. This is a well-established fact and is due to the electron correlation energy U_{eff} that affects the two-hole final states in core-resonant DPE.[41,42,52]

Near $E_B^{2e} = 0$, the intensity is close to zero and starts to increase around $E_B^{2e} = 3$ eV and levels off in the range $E_B^{2e} = 6-9$ eV. This is the range in which the signal originates from direct DPE. This is in line with previous DPE studies on Cu surfaces where the photon energy was not sufficient to excite the $3p$ level.[47–50] The direct DPE spectrum does exhibit such large energy shift as core-resonant DPE is in agreement with recent DPE studies from Ag and Pd surfaces study.[53] The latter revealed that such a shift has to be smaller than 0.2 eV.[53] Therefore, the direct DPE spectrum lies above the core-resonant part. We have labeled this region with the group symmetry designations of the Cu band structure.[54] If two electrons from the Δ_2' bands are emitted, then their final state lies energetically just above the position of the ^3F multiplet. This spectral range is bounded by the vertical dashed red lines. After the identification of the binding energy ranges of the two DPE pathways we want to look more closely at the difference spectrum in Fig. 3(b). If we were to proceed and add the entries for a given sum energy in analogy the E_{sum} spectrum, we will obtain essentially a zero result. This can be seen by observing the different color for the pockets A and B, which indicate a sign reversal. This in line with the theoretical prediction that states there is a sign reversal upon a grand reflection of the experiment.[7] This is a mirror operation along the bisecting line in Fig. 3(b). In order to obtain a nonvanishing result, we treat the data in Fig. 3(b) above and below the bisecting line separately. If the entries are above this line, we add those which belong to the same sum energy. This will provide a difference $(\sigma^+ - \sigma^+)$ spectrum as a function of the sum energy. The data below the bisecting line are treated the same way after sign reversal. This provides an additional difference curve, and we, finally, combine the two curves. The final result is the curve shown in Fig. 4(b).

As it was apparent from the 2D-energy plot of Fig. 3(a), the strongest effect occurs for the core-resonant path at $E_B^{2e} = 13.8$ eV, this is the position of the ^1G multiplet. At the energetic position of the ^3F term, the difference spectrum is zero. A weak signal from the direct DPE pathway becomes visible in the range of the Δ_2' part of the band structure.

An important difference between the ^1G and the ^3F state concerns their spin state, which is either a singlet or triplet state. The singlet state is antisymmetric upon exchange of the two electrons. Since the two-electron wave functions has to be antisymmetric upon exchange, we observe dichroism if the spatial wave functions of the two holes are symmetric with respect to exchange. There is no simple argument why the ^3F state shows no signal.

The two-electron dipole interaction with light conserves spins. Thus, the spin symmetry upon exchange of the initial and final two-electron states is the same. In other words, the transition is from a singlet (triplet) to singlet (triplet) state. For a symmetric

configuration (meaning, the two electron have the same energy and positioned symmetrically with respect to the incoming photon), the cross section vanishes and so does the chiral dichroism at this point. A finite cross section can still be detected in a solid state target due to multiple scattering events, which, however, may randomize the phases of the outcoming wave and, therefore, suppress the dichroism.

Besides the one-step description of the dichroism in DPE,[7,8] there exists also a work, which deals with the core-resonant pathway in the two-step picture.[12] A key difference of the two approaches is how the angle θ_{rel} between the trajectories of the two electrons enters in the calculation of the intensity. In a one-step process, the signal depends on $\sin(\theta_{rel})$, while in a two-step process, the term $\sin(2\theta_{rel})$ is relevant. The origin of this different behavior lies in the additional constraint of parity on the intermediate state in the two-step core-resonant DPE.[12] This has important implications for our geometric arrangement for which $\theta_{rel} = 90°$. Therefore, the observation of a dichroic signal in our geometry rules out a two-step process. This is an additional proof that the core-resonant DPE involving the Cu $3p$ level must be described within a one-step process.

IV. SUMMARY

We have investigated the DPE process from a Cu(100) surface upon excitation with circular polarized light. The photon energy is sufficient to ionize the $3p$ level, and, hence, the core-resonant and direct DPE processes can be observed. We adapted our instrument to be sensitive enough to detect a dichroic signal. We find a clear dichroism on the ^1G component of the Auger spectrum, while the ^3F component displays no dichroism. A part of the direct DPE spectrum associated with the Δ_2' bands also displays a dichroic signal. The geometry of the experiment ensures that only a one-step process of both DPE pathways can lead to dichroism.

Our results show that it is possible to imprint chirality onto the emitted electron pair through the incoming circular polarized photon in many electron systems.

AUTHOR DECLARATIONS
Conflict of Interest

The authors have no conflicts to disclose.

DATA AVAILABILITY

The data that support the findings of this study are available from the corresponding author upon reasonable request.

REFERENCES

[1] A. Einstein, Ann. Phys. **322**, 132 (1905).

[2] J. L. Powell and B. Crasemann, *Quantum Mechanics* (Dover, Mineola, NY, 2015).

[3] J. Berakdar, Phys. Rev. B **58**, 9808 (1998).

[4] N. Fominykh, J. Berakdar, J. Henk, and P. Bruno, Phys. Rev. Lett. **89**, 086402 (2002).

[5] O. Gunnarsson and K. Schönhammer, Phys. Rev. B **22**, 3710 (1980).

[6] F. Da Pieve, S. Di Matteo, D. Sébilleau, R. Gunnella, G. Stefani, and C. R. Natoli, Phys. Rev. A **75**, 052704 (2007).

[7] J. Berakdar and H. Klar, Phys. Rep. **340**, 473 (2001).

[8] J. Berakdar and H. Klar, Phys. Rev. Lett. **69**, 1175 (1992).

[9] J. Viefhaus *et al.* Phys. Rev. Lett. **77**, 3975 (1996).

[10] K. Soejima, A. Danjo, K. Okuno, and A. Yagishita, Phys. Rev. Lett. **83**, 1546 (1999).

[11] M. Achler, V. Mergel, L. Spielberger, R. Dörner, Y. Azuma, and H. Schmidt-Böcking, J. Phys. B: At., Mol. Opt. Phys. **34**, 965 (2001).

[12] N. M. Kabachnik and V. Schmidt, J. Phys. B: At., Mol. Opt. Phys. **28**, 233 (1995).

[13] G. A. van Riessen, Z. Wei, R. S. Dhaka, C. Winkler, F. O. Schumann, and J. Kirschner, J. Phys.: Condens. Matter **22**, 092201 (2010).

[14] F. O. Schumann, R. S. Dhaka, G. A. van Riessen, Z. Wei, and J. Kirschner, Phys. Rev. B **84**, 125106 (2011).

[15] G. A. van Riessen, F. O. Schumann, M. Birke, C. Winkler, and J. Kirschner, J. Phys.: Conf. Ser. **185**, 012051 (2009).

[16] G. A. van Riessen, F. O. Schumann, M. Birke, C. Winkler, and J. Kirschner, J. Phys.: Condens. Matter **20**, 442001 (2008).

[17] S. Thurgate, Surf. Interface Anal. **20**, 627 (1993).

[18] W. Bothe and H. Geiger, Zeitschrift für Physik **32**, 639–663 (1925).

[19] I. E. McCarthy and E. Weigold, Phys. Rep. **27**, 275 (1976).

[20] P. Calicchia, S. Lagomarsino, F. Scarinci, C. Martinelli, and V. Formoso, Rev. Sci. Instrum. **70**, 3529 (1999).

[21] E. M. Purcell, Phys. Rev. **54**, 818 (1938).

[22] R. E. Imhof, A. Adams, and G. C. King, J. Phys. E **9**, 138 (1976).

[23] K. J. S. Sawhney, F. Senf, M. Scheer, F. Schäfers, J. Bahrdt, A. Gaupp, and W. Gudat, Nucl. Instrum. Methods Phys. Res., Sect. A **390**, 395 (1997).

[24] M. R. Weiss *et al.*, Nucl. Instrum. Methods Phys. Res., Sect. A **467–468**, 449 (2001).

[25] R. Gotter, A. Ruocco, M. T. Butterfield, S. Iacobucci, G. Stefani, and R. A. Bartynski, Phys. Rev. B **67**, 033303 (2003).

[26] R. Gotter, F. Da Pieve, A. Ruocco, F. Offi, G. Stefani, and R. A. Bartynski, Phys. Rev. B **72**, 235409 (2005).

[27] Z. Wei, F. O. Schumann, C. H. Li, L. Behnke, G. Di Filippo, G. Stefani, and J. Kirschner, Phys. Rev. Lett. **113**, 267603 (2014).

[28] I. Kostanovskiy, F. O. Schumann, Y. Aliaev, Z. Wei, and J. Kirschner, J. Phys.: Condens. Matter **28**, 015601 (2016).

[29] J. F. Moulder, W. F. Stickle, P. E. Sobol, and K. D. Bomben, *Handbook of X-ray Photoelectron Spectroscopy* (Perkin-Elmer, Eden Prairie, MN, 1992).

[30] NIST X-ray Photoelectron Spectroscopy Database, Version 4.1, National Institute of Standards and Technology, Gaithersburg, 2012.

[31] S. Hüfner, *Photoelectron Spectroscopy* (Springer, Berlin, 2003).

[32] G. Di Filippo, *et al.*, J. Phys.: Condens. Matter **27**, 085003 (2015).

[33] G. Di Filippo, F. O. Schumann, S. Patil, Z. Wei, G. Stefani, G. Fratesi, M. I. Trioni, and J. Kirschner, J. Electron. Spectrosc. Relat. Phenom. **211**, 32 (2016).

[34] T. Leitner *et al.*, J. Electron. Spectrosc. Relat. Phenom. **250**, 147075 (2021).

[35] A. Born, T. Leitner, I. Bidermane, R. Ovsyannikov, S. Svensson, N. Mårtensson, and A. Föhlisch, Phys. Rev. B **103**, 115121 (2021).

[36] G. Wendin, *Breakdown of the One Electron Pictures in Photoelectron Spectra* (Springer, Berlin, 1981).

[37] B. D. Napitu and J. Berakdar, Phys. Rev. B **81**, 195108 (2010).

[38] F. O. Schumann, Y. Aliaev, I. Kostanovskiy, G. Di Filippo, Z. Wei, and J. Kirschner, Phys. Rev. B **93**, 235128 (2016).

[39] F. O. Schumann, J. Kirschner, and J. Berakdar, Phys. Status Solidi B **257**, 1900636 (2020).

[40] G. A. Sawatzky, Phys. Rev. Lett. **39**, 504 (1977).

[41] E. Antonides, E. C. Janse, and G. A. Sawatzky, Phys. Rev. B **15**, 1669 (1977).

[42] A. C. Parry-Jones, P. Weightman, and P. T. Andrews, J. Phys. C: Solid State Phys. **12**, 1587 (1979).

[43] M. Cini, Solid State Commun. **24**, 681 (1977).

[44] K. D. Childs, B. A. Carlson, L. A. LaVenier, J. F. Moulder, D. F. Paul, W. F. Stickle, and D. G. Watson, *Handbook of Auger Electron Spectroscopy* (Physical Electronics, Eden Prairie, 1995).

[45] C. Roth, F. Hillebrecht, H. Rose, and E. Kisker, Phys. Rev. Lett. **70**, 3479 (1993).

[46] R. Gotter, F. Da Pieve, F. Offi, A. Ruocco, A. Verdini, H. Yao, R. Bartynski, and G. Stefani, Phys. Rev. B **79**, 075108 (2009).

[47] F. O. Schumann, C. Winkler, and J. Kirschner, Phys. Rev. Lett. **98**, 257604 (2007).

[48] F. O. Schumann, N. Fominykh, C. Winkler, J. Kirschner, and J. Berakdar, Phys. Rev. B **77**, 235434 (2008).

[49] A. Trützschler, M. Huth, C.-T. Chiang, R. Kamrla, F. O. Schumann, J. Kirschner, and W. Widdra, Phys. Rev. Lett. **118**, 136401 (2017).

[50] F. O. Schumann and J. Kirschner, Phys. Rev. B **103**, 085435 (2021).

[51] G. A. Sawatzky, "Auger photoelectron coincidence spectroscopy," in *Auger Electron Spectroscopy*, edited by C. L. B. R. P. Messmer (Academic, San Diego, 1988).

[52] H. W. Haak, G. A. Sawatzky, and T. D. Thomas, Phys. Rev. Lett. **41**, 1825 (1978).

[53] F. O. Schumann, Y. Aliaev, I. Kostanovskiy, and J. Kirschner, Phys. Rev. B **101**, 115104 (2020).

[54] U. Rücker, H. Gollisch, and R. Feder, Phys. Rev. B **72**, 214424 (2005).